Pergamon

Int. J. Solids Structures Vol. 35, No. 7–8, pp. 619–635, 1998

0020–7683/98 $19.00 + .00

PII: S0020–7683(97)00065–6

A COMPREHENSIVE ANALYSIS OF THE DYNAMICS OF A HELICOPTER ROTOR BLADE

M. R. M. CRESPO DA SILVA
Department of Mechanical Engineering, Aeronautical Engineering and Mechanics, Rensselaer Polytechnic Institute, Troy, NY 12180-3590, U.S.A.

(*Received* 3 *August* 1996; *in revised form* 27 *February* 1997)

Abstract—A comprehensive and versatile analysis of the response of a helicopter rotor blade is presented in this paper. First, the full nonlinear partial differential equations that govern the motion of the blade, taking into account the geometrical nonlinearities that arise due to deformation, are presented. The equilibrium solution exhibited by the system is then determined using a relatively simple model for the aerodynamic forces, common in the rotorcraft dynamics literature. The equilibrium solution is determined by numerical integration of a nonlinear two-point boundary value problem. The blade's equilibrium is then perturbed and the stability of infinitesimally small perturbations is analyzed in detail. The analysis presented here yields essentially exact results for the equilibrium solution and for the eigenvalues and eigenfunctions associated with the infinitesimally small perturbations about the equilibrium. © 1997 Elsevier Science Ltd

INTRODUCTION

The investigation of the response of a rotor blade includes the determination of a particular solution to the differential equations of motion of the system and the analysis of the perturbed motion about the particular solution. For the case of hover, the particular solution is an equilibrium (i.e. constant in time) solution. For this case, the investigation of the perturbed motion includes the determination of the eigenvalues associated with infinitesimally small motions about the equilibrium solution (or solutions). Because of the complexity of the governing differential equations of motion, it has been common practice in the rotorcraft dynamics literature to first expand the full nonlinear differential equations, to a pre-determined degree in a small parameter, about the undeformed state of the system. The resulting differential equations, which contain polynomial nonlinearities truncated to the desired order, are then used to analyze the aeroelastic response of the blade. Since the undeformed state is not an equilibrium solution to the full nonlinear differential equations of motion, one must be careful when using such expanded equations in order to obtain results that are consistent with the approximating assumptions. As shown in Crespo da Silva *et al.* (1991) for a cantilever with a tip mass, even a cubic approximation to such equations may yield, in some cases, very inaccurate eigenvalues for the perturbed linearized motion. As pointed out in that reference, the mathematically correct way to expand the full nonlinear differential equations of motion is, of course, to always expand them about a particular solution (such as an equilibrium solution) exhibited by such equations.

An analysis of the response of a rotor blade in hover was presented in Crespo da Silva and Hodges (1986a, 1986b) by making use of Galerkin's method with a set of eigenfunctions for a non-rotating beam. In such methodology, the number of Galerkin coefficients depends on the number of eigenfunctions used and on the order of truncation of the expanded differential equations of motion. As shown in the second of the references mentioned above, such a number is greatly increased when one increases the truncation order of the expanded equations from quadratic [see, for example Hodges and Dowell (1974), Hodges and Ormiston (1976)] to cubic.

In this paper, the problem of determining the equilibrium solution and the eigenvalues associated with the perturbed, infinitesimally small, aeroelastic response of a helicopter rotor blade in hover is analyzed in a mathematically exact manner. First, the equilibrium state is determined directly by numerically solving the two-point boundary value problem

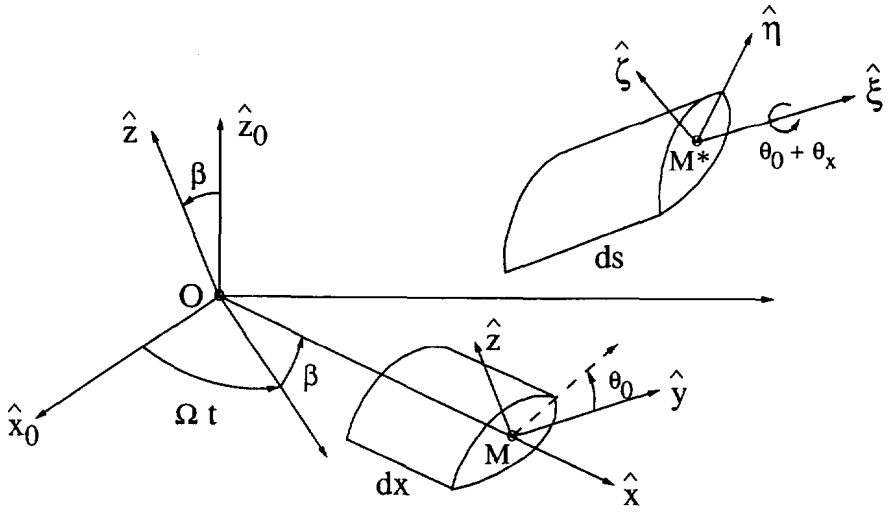

Fig. 1. A segment of a rotor blade.

associated with the original nonlinear differential equations of motion that govern the blade's response. An approach based on the general form of the solution to linearized differential equations of motion is then used for determining the eigenfunctions and the eigenvalues associated with such perturbations, thus, eliminating the need to use approximate methods to do so.

NONLINEAR DIFFERENTIAL EQUATIONS OF MOTION

The differential equations governing the nonlinear flexural-flexural-torsional dynamics of beams, taking into account the geometric nonlinearities in the system in a mathematically consistent manner, were formulated in Crespo da Silva and Glynn (1978a) for inextensional beams. That work was generalized to account for extensionality [e.g. Crespo da Silva (1988)], and for the effects that arise from mounting the beam in a rotating base [e.g. Crespo da Silva (1991)], as in the case of a helicopter rotor blade. The differential equations generated from the formulation presented in Crespo da Silva (1991) are used here to investigate the response, and its stability, of a helicopter rotor blade in hover by making use of a rigorous analysis methodology that is applicable to all dynamical systems. The results obtained are essentially exact.

The system considered here is a helicopter rotor. It consists of $N > 2$ initially straight and untwisted identical helicopter rotor blades of undeformed length R, pre-cone angle β and collective pitch angle θ_0. Both β and θ_0 are constants. Each blade is modeled as a beam, which is cantilevered to the rotating rotor. The rotor is spinning with a constant angular velocity Ω about a fixed direction in space and is attached to a helicopter in hover.

A blade segment, before and after deformation, is shown in Fig. 1 (the quantities with a caret, such as $\hat{x}$, $\hat{\eta}$, etc, are unit vectors). Point O in that figure is inertial since the helicopter is in hover. The small offset between O and the blade's root, which exists in practice, is neglected in this model. The unit vectors $\hat{x}_0$ and $\hat{z}_0$ shown in Fig. 1 are inertial, and $\hat{z}$ is parallel to $\hat{z}_0$ if $\beta = 0$. The unit vectors $\hat{\xi}$, $\hat{\eta}$ and $\hat{\zeta}$ are parallel to the principal directions of the blade's cross-section at M^*, where M^* is the location of the cross-section reference point M after the blade undergoes elastic deformation. The blade's cross-section is symmetric about the η axis and is shaped with an aerodynamic profile; it is assumed that its area and mass centroids, and aerodynamic center, coincide at M^*.

The blade is modeled as a modified Euler–Bernoulli beam for which shear effects are neglected and the small effect of warping in the ξ-direction (see Fig. 1) is taken into account only in the calculation of the blade's torsional stiffness [see Crespo da Silva (1988) for details]. The orientation of the cross-section triad $(\hat{\xi}, \hat{\eta}, \hat{\zeta} = \hat{\xi} \times \hat{\eta})$ relative to the rotating triad $(\hat{x}, \hat{y}, \hat{z} = \hat{x} \times \hat{y})$ can be described with the three-axis rotation sequence

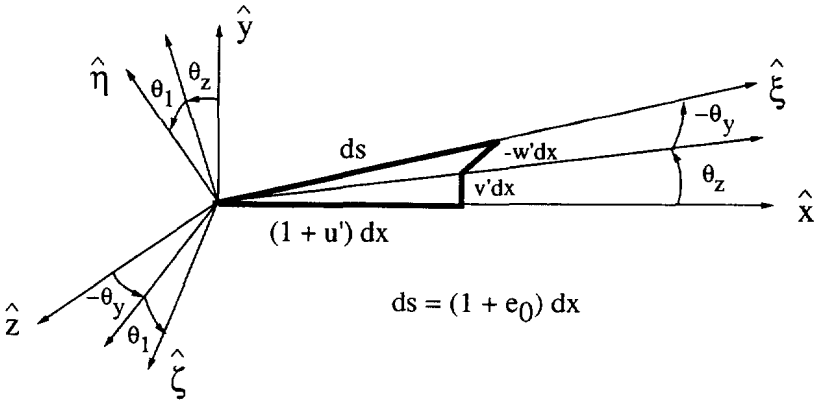

Fig. 2. Orientation angles and the elastic displacements.

$\theta_z, -\theta_y, \theta_1 = \theta_0 + \theta_x$ shown in Fig. 2. The angle θ_y used here is the negative of a similar angle that appear in Crespo da Silva (1991); with this convention, a positive value for θ_y conveniently implies a positive value for the "flap deflection" w (which is the actual deflection normalized by R). With this rotation sequence, the angles θ_z and θ_y are related to the non-dimensional components u, v and w of the elastic deformation vector R $(u\hat{x}+v\hat{y}+w\hat{z})$ associated with the reference point M^* as shown in eqn (1) below (see Fig. 2). The flap deflection w and the "lead-lag deflection" v are the components due to bending. As shown in Figs 1 and 2, the blade's reference point M^* leads the rotating reference axis OM when v is positive and lags it otherwise.

$$\begin{aligned} v' &= (1+e_0)\cos\theta_y \sin\theta_z \\ w' &= (1+e_0)\sin\theta_y \\ 1+u' &= (1+e_0)\cos\theta_y \cos\theta_z. \end{aligned} \tag{1}$$

Here, primes denote partial differentiation with respect to the non-dimensional spatial variable $x = |\overrightarrow{OM}|/R$, which is distance along the rotating undeformed blade's reference axis, normalized by R. Also, according to Fig. 1 and eqn (1), the quantity e_0 is equal to $e_0 = \partial s/\partial x - 1 = \sqrt{(1+u')^2+v'^2+w'^2} - 1$; e_0 is a very small quantity and it is equal to zero for inextensional beams.

The components of the unit vector triads $(\hat{\xi}, \hat{\eta}, \hat{\zeta})$ and $(\hat{x}, \hat{y}, \hat{z})$ are related as

$$\begin{bmatrix} \hat{\xi} \\ \hat{\eta} \\ \hat{\zeta} \end{bmatrix} = T \begin{bmatrix} \hat{x} \\ \hat{y} \\ \hat{z} \end{bmatrix}.$$

The elements T_{ij} of the transformation matrix T are given below since they appear in several equations in this paper. In the following expressions, $\theta_1 = \theta_0 + \theta_x$.

$$T = \begin{bmatrix} \cos\theta_y \cos\theta_z & \cos\theta_y \sin\theta_z & \sin\theta_y \\ -\sin\theta_z \cos\theta_1 - \sin\theta_y \cos\theta_z \sin\theta_1 & \cos\theta_z \cos\theta_1 - \sin\theta_y \sin\theta_z \sin\theta_1 & \cos\theta_y \sin\theta_1 \\ \sin\theta_z \sin\theta_1 - \sin\theta_y \cos\theta_z \cos\theta_1 & -\cos\theta_z \sin\theta_1 - \sin\theta_y \sin\theta_z \cos\theta_1 & \cos\theta_y \cos\theta_1 \end{bmatrix}. \tag{2}$$

The expression for the deformed blade's curvature vector $\mathbf{C}$ (normalized by $1/R$, and including the torsion) and for the absolute (i.e. relative to inertial space) angular velocity vector $\boldsymbol{\omega}$ of the blade's cross-section (normalized by Ω) are given below [see Crespo da Silva (1991) for the details of the derivations]. Overdots denote partial differentiation with

respect to normalized time $\tau = \Omega t$, where t denotes dimensional time, and $\triangleq$ means "equal to by definition".

$$\begin{aligned}
\mathbf{C} &= (\theta_x' + \theta_z' \sin\theta_y)\hat{\xi} + (\theta_z' \sin\theta_1 \cos\theta_y - \theta_y' \cos\theta_1)\hat{\eta} + (\theta_z' \cos\theta_1 \cos\theta_y + \theta_y' \sin\theta_1)\hat{\zeta} \\
&\triangleq C_\xi \hat{\xi} + C_\eta \hat{\eta} + C_\zeta \hat{\zeta} \\
\boldsymbol{\omega} &= [\dot{\theta}_x + (\dot{\theta}_z + \cos\beta)\sin\theta_y + \sin\beta\cos\theta_y\cos\theta_z]\hat{\xi} \\
&\quad + [(\dot{\theta}_z + \cos\beta)\sin\theta_1\cos\theta_y - \dot{\theta}_y\cos\theta_1 - (\cos\theta_1\sin\theta_z + \sin\theta_1\sin\theta_y\cos\theta_z)\sin\beta]\hat{\eta} \\
&\quad + [(\dot{\theta}_z + \cos\beta)\cos\theta_1\cos\theta_y + \dot{\theta}_y\sin\theta_1 + (\sin\theta_1\sin\theta_z - \cos\theta_1\sin\theta_y\cos\theta_z)\sin\beta]\hat{\zeta} \\
&\triangleq \omega_\xi \hat{\xi} + \omega_\eta \hat{\eta} + \omega_\zeta \hat{\zeta}. \qquad (3)
\end{aligned}$$

The blade's elastic angle of twist, $\phi(x, \tau)$, is found as

$$\phi(x,\tau) = \int_0^x C_\xi(\eta,\tau)\,\mathrm{d}\eta = \theta_x(x,\tau) + \int_0^x \theta_z'(\eta,\tau)\sin\theta_y(\eta,\tau)\,\mathrm{d}\eta. \qquad (4)$$

The differential equations of motion for the blade and a boundary condition equation, are formulated following the approach presented in Crespo da Silva (1991, 1988). For simplicity, a homogeneous blade of constant distributed mass m kg m^{-1} is considered. The four normalized differential equations of motion involving the four non-dimensional variables u, v, w and θ_x are obtained as [e.g. Crespo da Silva (1991)]

$$\begin{aligned}
G_u' &\triangleq \left[A_{\theta_z}\frac{\partial\theta_z}{\partial u'} + A_{\theta_y}\frac{\partial\theta_y}{\partial u'} + \lambda(1+u')\right]' = f_u \\
G_v' &\triangleq \left[A_{\theta_z}\frac{\partial\theta_z}{\partial v'} + A_{\theta_y}\frac{\partial\theta_y}{\partial v'} + \lambda v'\right]' = \ddot{v} + 2\dot{u}\cos\beta - 2\dot{w}\sin\beta - v - Q_v \\
G_w' &\triangleq \left[A_{\theta_z}\frac{\partial\theta_z}{\partial w'} + A_{\theta_y}\frac{\partial\theta_y}{\partial w'} + \lambda w'\right]' = \ddot{w} + 2\dot{v}\sin\beta - w\sin^2\beta + \frac{1}{2}(x+u)\sin 2\beta - Q_w \\
&\quad - \{[D_\xi + e_0(D_\eta + D_\zeta)]C_\xi\}' + (D_\eta - D_\zeta)C_\eta C_\zeta + J_\xi\dot{\omega}_\xi - (J_\eta - J_\zeta)\omega_\eta\omega_\zeta = Q_{\theta_x} \qquad (5)
\end{aligned}$$

where $f_u = \ddot{u} - 2\dot{v}\cos\beta + w(\sin 2\beta)/2 - (x+u)\cos^2\beta - Q_u$, while Q_u, Q_v, Q_w and Q_{θ_x} are the normalized generalized forces whose specific (i.e. per unit length) virtual work is $m\Omega^2R^2(Q_u\delta u + Q_v\delta v + Q_w\delta w + Q_{\theta_x}\delta\theta_x)$. The expressions for A_{θ_z} and A_{θ_y} are [e.g. Crespo da Silva (1991), with θ_y replaced by $-\theta_y$ in that reference].

$$\begin{aligned}
A_{\theta_z} &= -\{[D_\xi + e_0(D_\eta + D_\zeta)]C_\xi T_{13} + D_\eta C_\eta T_{23} + D_\zeta C_\zeta T_{33}\}' \\
&\quad + [J_\xi\omega_\xi T_{13} + J_\eta\omega_\eta T_{23} + J_\zeta\omega_\zeta T_{33}]^{\cdot} + (J_\xi\omega_\xi T_{12} + J_\eta\omega_\eta T_{22} + J_\zeta\omega_\zeta T_{32})\sin\beta \\
A_{\theta_y} &= [D_\eta C_\eta\cos\theta_1 - D_\zeta C_\zeta\sin\theta_1]' - [J_\eta\omega_\eta\cos\theta_1 - J_\zeta\omega_\zeta\sin\theta_1]^{\cdot} \\
&\quad + \{[D_\xi + e_0(D_\eta + D_\zeta)]C_\xi\cos\theta_y - [D_\eta C_\eta\sin\theta_1 + D_\zeta C_\zeta\cos\theta_1]\sin\theta_y\}\theta_z' \\
&\quad - \omega_\xi[J_\eta\omega_\zeta\cos\theta_1 + J_\zeta\omega_\eta\sin\theta_1] - \dot{\theta}_1[J_\eta\omega_\eta\sin\theta_1 + J_\zeta\omega_\zeta\cos\theta_1] \qquad (6)
\end{aligned}$$

The following boundary condition equation is obtained from the variational formulation that yields eqn (5), where δW_{B} is the contribution (if any) to such equation from the virtual work of the nonpotential forces.

$$\Big[D_\xi C_\xi \delta\theta_x + G_u\delta u + G_v\delta v + G_w\delta w - H_u\delta u' - H_v\delta v'$$

$$- \frac{1}{1+e_0}[D_\eta C_\eta \cos\theta_1 - D_\zeta C_\zeta \sin\theta_1](\cos\theta_y)\delta w'\Big]_{x=0}^{1} - \delta W_B = 0. \quad (7)$$

In the above equation, H_u and H_v are given by

$$H_u = \frac{1}{1+e_0}\{[D_\zeta C_\zeta \sin\theta_1 - D_\eta C_\eta \cos\theta_1]\sin\theta_y \cos\theta_z$$
$$+ [D_\xi + e_0(D_\eta + D_\zeta)]C_\xi \tan\theta_y \sin\theta_z + [D_\eta C_\eta \sin\theta_1 + D_\zeta C_\zeta \cos\theta_1]\sin\theta_z\}$$
$$H_v = \frac{1}{1+e_0}\{[D_\zeta C_\zeta \sin\theta_1 - D_\eta C_\eta \cos\theta_1]\sin\theta_y \sin\theta_z$$
$$- [D_\xi + e_0(D_\eta + D_\zeta)]C_\xi \tan\theta_y \cos\theta_z - [D_\eta C_\eta \sin\theta_1 + D_\zeta C_\zeta \cos\theta_1]\cos\theta_z\}. \quad (8)$$

In the above equations, D_η and D_ζ are the blade's bending stiffnesses, and D_ξ is the torsional stiffness, all normalized by $m\Omega^2R^4$. The quantities J_η, J_ζ and J_ξ are the blade's distributed mass moments of inertia, normalized by mR^2. The quantity λ that appears in the first three of eqn (5) is equal to

$$\lambda = \frac{EAe_0 + (D_\eta + D_\zeta)C_\xi^2/2}{1+e_0}, \quad (9)$$

where EA is the blade's axial stiffness, normalized by $m\Omega^2R^2$.

By making use of eqn (9), the second and third of eqn (5) can be reduced to two integro-differential forms with G_v and G_w as shown below.

$$G_v = \frac{A_{\theta_z}}{(1+e_0)\cos\theta_y\cos\theta_z} + (\tan\theta_z)\int_1^x f_u\,dx$$
$$G_w = (\sin\theta_z\tan\theta_y)G_v + \frac{A_{\theta_y}}{(1+e_0)\cos\theta_y} + (\tan\theta_y\cos\theta_z)\int_1^x f_u\,dx \quad (10)$$

The generalized forces that appear in the differential equations of motion are given in the next section.

GENERALIZED AERODYNAMIC FORCES

In this paper, the aerodynamic forces and moments are modeled using the relatively simple quasi-steady strip theory based on Greenberg's extension of Theodorsen's theory in which only the $\hat\eta$ and $\hat\zeta$ components of the velocity of point M^* in the blade's reference axis (see Fig. 1) relative to the air are taken into account in the calculation of the aerodynamic load, as done in Hodges and Ormiston (1976), and Peters (1975), for example. By taking into account the induced airflow through the rotor blade assembly, whose absolute velocity is equal to $-\Omega R v_i \hat z_0$ (see Fig. 1), the velocity of point M^* relative to the air is

$$\mathbf{v}_{M^*/\text{air}} = \Omega R\{[\dot u - v\cos\beta + v_i\sin\beta]\hat x + [\dot v + (x+u)\cos\beta - w\sin\beta]\hat y$$
$$+ [\dot w + v\sin\beta + v_i\cos\beta]\hat z\} \triangleq \Omega R(v_x\hat x + v_y\hat y + v_z\hat z). \quad (11)$$

According to the aerodynamic theory being used here, the specific aerodynamic force $\mathbf{F}_{\text{aero}}$ (normalized by $m\Omega^2R$) and moment $\mathbf{M}_{\text{aero}}$ (normalized by $m\Omega^2R^2$) are given as [e.g. Crespo da Silva and Hodges (1986b); Peters (1975)]

$$\mathbf{F}_{\text{aero}} = \frac{\gamma}{6}\left\{\left[v_\zeta\left(v_\zeta - \frac{c}{2}\omega_\xi\right) - \frac{c_{d0}}{2\pi}Uv_\eta\right]\hat{\eta} - \left[v_\eta\left(v_\zeta - \frac{c}{2}\omega_\xi\right) + \frac{c_{d0}}{2\pi}Uv_\zeta + \frac{c}{4}\left(\dot{v}_\zeta - \frac{c}{4}\dot{\omega}_\xi\right)\right]\hat{\zeta}\right\}$$

$$\triangleq F_\eta\hat{\eta} + F_\zeta\hat{\zeta}$$

$$\mathbf{M}_{\text{aero}} = -\frac{\gamma c^2}{96}\left[U\omega_\xi - \dot{v}_\zeta + \frac{3}{8}\dot{\omega}_\xi\right]\hat{\xi} \triangleq M_{\text{aero}}\hat{\xi}. \tag{12}$$

In the above equations, c is the airfoil's chord normalized by R, c_{d0} is the airfoil's profile drag coefficient, $\gamma = 6\pi R^2 c\rho_{\text{air}}/m$ (which is called the *Lock number* for the blade) where ρ_{air} is the air density, and $U = \sqrt{v_\eta^2 + v_\zeta^2}$. The quantities v_η and v_ζ are the $\hat{\eta}$ and $\hat{\zeta}$ components of the velocity $\boldsymbol{v}_{M^*/\text{air}}$ of M^* relative to the air. They are related to v_x, v_y and v_z as shown in eqn (13) given below.

$$\begin{aligned} v_\eta &= T_{21}v_x + T_{22}v_y + T_{23}v_z \\ v_\zeta &= T_{31}v_x + T_{32}v_y + T_{33}v_z. \end{aligned} \tag{13}$$

The expressions for the normalized generalized forces Q_u, Q_v, Q_w and $Q_{\theta x}$ are extracted directly from the expression for the virtual work $(\delta W)_{\text{aero}}$ done by the aerodynamic forces acting on the blade, which is equal to

$$(\delta W)_{\text{aero}} = \int_0^1 \{F_x\delta u + F_y\delta v + F_z\delta w + M_{\text{aero}}[\delta\theta_x + (\sin\theta_y)\delta\theta_z]\}\,\mathrm{d}x$$

$$\triangleq \delta W_{\text{B}} + \int_0^1 [Q_u\delta u + Q_v\delta v + Q_w\delta w + Q_{\theta_x}\delta\theta_x]\,\mathrm{d}x \tag{14}$$

where

$$\begin{aligned} F_x &= T_{21}F_\eta + T_{31}F_\zeta \\ F_y &= T_{22}F_\eta + T_{32}F_\zeta \\ F_z &= T_{23}F_\eta + T_{33}F_\zeta \end{aligned} \tag{15}$$

are the components of $\mathbf{F}_{\text{aero}}$ in the $\hat{x}$, $\hat{y}$ and $\hat{z}$-directions, respectively (see Fig. 1).

This gives the following expressions for the specific generalized forces that are needed in eqn (5), and for δW_{B}, which appears in the boundary condition equation, eqn (7). The effect of the generalized gravitational forces are neglected when compared to the generalized aerodynamic forces, as customarily done in the rotorcraft literature.

$$Q_u = F_x - \left[M_{\text{aero}}\frac{\partial\theta_z}{\partial u'}\sin\theta_y\right]' = F_x + \left[\frac{M_{\text{aero}}(\sin\theta_z)\tan\theta_y}{1+e_0}\right]'$$

$$Q_v = F_y - \left[M_{\text{aero}}\frac{\partial\theta_z}{\partial v'}\sin\theta_y\right]' = F_y - \left[\frac{M_{\text{aero}}(\cos\theta_z)\tan\theta_y}{1+e_0}\right]'$$

$$Q_w = F_z$$

$$Q_{\theta_x} = M_{\text{aero}}$$

$$\delta W_{\text{B}} = \left\{M_{\text{aero}}\left[\frac{\partial\theta_z}{\partial u'}\delta u + \frac{\partial\theta_z}{\partial v'}\delta v\right]\sin\theta_y\right\}_{x=0}^{1}. \tag{16}$$

To complete the formulation of the problem, we now need to have an expression to determine the normalized velocity v_i of the induced airflow through the rotor blade assembly. For this, a simple model is also used where v_i is approximated as a constant determined by using momentum theory [e.g. Bramwell (1976); Peters (1975)] as $v_i = \sqrt{C_T/2}$, with C_T being the normalized average rotor thrust coefficient given by (see Fig. 1)

$$C_T = \frac{\text{average rotor thrust}}{\pi R^2 \rho_{air}(\Omega R)^2} = \frac{\frac{b}{2\pi}}{\pi R^2 \rho_{air}(\Omega R)^2} \int_0^{2\pi} \int_0^1 (m\Omega^2 R F_z \hat{z} \bullet \hat{z}_0)\, \mathrm{d}(Rx)\, \mathrm{d}\tau \tag{17}$$

where b is the number of blades in the rotor system.

To evaluate the above integral, the same approximation used in Peters (1975) is used here, namely, that C_T has a slow reaction time compared to one rotor revolution so that the equilibrium values for $F_z(x)$ are used in the integrand. With this approximation, the following expression is then obtained for C_T. The subscript e attached to a variable is used in this paper to denote the equilibrium value for that variable.

$$C_T \approx \frac{6bc \cos\beta}{\gamma} \int_0^1 Q_{we}\, \mathrm{d}x. \tag{18}$$

This completes the formulation of the basic equations that are necessary to investigate the dynamics of the rotor blade. The equilibrium response and the stability of the perturbed motion about the equilibrium are investigated in the next section.

ANALYSIS OF THE MOTION

The boundary conditions for the rotor blade are extracted from eqn (7). The boundary conditions at $x = 0$ correspond to $\delta\alpha = 0$, for $\alpha = u$, v, w, θ_x, θ_y and θ_z. The boundary conditions at $x = 1$ are obtained by equating to zero the coefficients of the virtual variations that appear in that equation. The boundary conditions are then as follows.

At $x = 0$

$$u = v = w = \theta_x = \theta_y = \theta_z = 0.$$

At $x = 1$

$$C_\xi = C_\eta = C_\zeta = G_w = 0$$

$$G_u = M_{aero} \frac{\partial \theta_z}{\partial u'} \sin\theta_y = -\frac{M_{aero}(\sin\theta_z)\tan\theta_y}{1+e_0}$$

$$G_v = M_{aero} \frac{\partial \theta_z}{\partial v'} \sin\theta_y = \frac{M_{aero}(\cos\theta_z)\tan\theta_y}{1+e_0}.$$

To integrate the equations of motion, we choose, for convenience, to use the first of eqn (5) and the boundary conditions associated with G_u to obtain a second expression for the quantity λ that appears in that equation. This yields

$$\lambda = \frac{1}{1+u'}\left[\int_1^x f_u(\eta,\tau)\, \mathrm{d}\eta - A_{\theta_z}\frac{\partial\theta_z}{\partial u'} - A_{\theta_y}\frac{\partial\theta_y}{\partial u'} - \frac{M_{aero}(\sin\theta_z)\tan\theta_y}{1+e_0}\right]. \tag{19}$$

When combined, the two expressions for λ given by eqns (9) and (19) yield the following relation that involves the elastic displacements u, v, w and their temporal and spatial partial derivatives.

$$e_0 = \frac{\left\{\dfrac{1}{\cos\theta_y \cos\theta_z}\left[\displaystyle\int_1^x f_u(\eta,\tau)\,\mathrm{d}\eta - A_{\theta_z}\frac{\partial\theta_z}{\partial u'} - A_{\theta_y}\frac{\partial\theta_y}{\partial u'} - \frac{M_{\text{aero}}(\sin\theta_z)\tan\theta_y}{1+e_0}\right] - \dfrac{D_\eta + D_\zeta}{2}C_\xi^2\right\}}{EA}. \tag{20}$$

Equation (20) clearly discloses that $e_0 \to 0$ as $EA \to \infty$ and, in the limit, the blade is inextensional. For long beams and actual rotor blades, EA is a finite, but large, quantity and, therefore, the blade will behave as essentially inextensional since, according to eqn (20), e_0 is a very small quantity. Based on this observation, a simpler approximation to eqn (20), which includes small terms only to the order of the blade's transverse deflections in the numerator of eqn (20), will be used to account for the very small non-zero value of e_0 in the calculations presented below. Therefore, for convenience, e_0 is approximated as shown in eqn (21) below.

$$e_0 \approx \frac{1}{EA}\left\{\int_1^x \left[\frac{w}{2}\sin 2\beta - 2\dot{v}\cos\beta - x\cos^2\beta\right]\mathrm{d}x\right\}. \tag{21}$$

In summary, the differential equations for the blade consist of the last three of eqn (5), with G_v and G_w given by eqn (10) and e_0 approximated as shown in eqn (21).

A direct mathematical approach is now used here to analyze the motion of the blade. First, the equilibrium solution for the system, for which the elastic deflections are not a function of time (but only a function of the independent variable x), is determined directly by numerical integration of the nonlinear ordinary differential equations that result from eqn (5) with the cantilever boundary conditions. For this, it is convenient to write the differential equations of motion in state variable form as

$$\underline{y}' = \underline{f}(\underline{y}, \dot{\underline{y}}, \ddot{\underline{y}}, \underline{y}', \ddot{\underline{y}}'), \tag{22}$$

where $\underline{y}$ is a 15×1 column matrix of state variables whose components are defined as

$$y_1 = v; y_2 = w; y_3 = \theta_z; y_4 = \theta_y; y_5 = \theta_x$$

$$y_6 = u = \int_0^x [(1+e_0)(\cos\theta_y)\cos\theta_z - 1]\,\mathrm{d}x; y_7 = \int_0^x C_\xi\,\mathrm{d}x$$

$$y_8 = [D_\xi + e_0(D_\eta + D_\zeta)]C_\xi; y_9 = e_0 \approx \frac{1}{EA}\int_1^x \left[\frac{w}{2}\sin 2\beta - 2\dot{v}\cos\beta - x\cos^2\beta\right]\mathrm{d}x$$

$$y_{10} = (D_\eta C_\eta \sin\theta_1 + D_\zeta C_\zeta \cos\theta_1)\cos\theta_y + [D_\xi + e_0(D_\eta + D_\zeta)]C_\xi \sin\theta_y$$

$$y_{11} = D_\eta C_\eta \cos\theta_1 - D_\zeta C_\zeta \sin\theta_1; y_{12} = \int_1^x f_u\,\mathrm{d}x$$

$$y_{13} = G_v; y_{14} = G_w; y_{15} = \int_x^1 \left[\frac{x+u}{2}\sin 2\beta - w\sin^2\beta\right]\mathrm{d}x. \tag{23}$$

The integro-partial differential equations of motion developed here are, then, equivalent to the following set of first-order nonlinear partial differential equations

$$y_1' = (1+y_9)(\sin y_3)\cos y_4$$

$$y_2' = (1+y_9)\sin y_4$$

$$\begin{bmatrix} y_3' \\ y_4' \end{bmatrix} = \frac{1}{\cos y_4}\begin{bmatrix} \dfrac{D_\zeta \sin^2\theta_1 + D_\eta \cos^2\theta_1}{D_\eta \cos y_4} & \dfrac{D_\zeta - D_\eta}{2D_\eta}\sin 2\theta_1 \\ -\dfrac{D_\zeta - D_\eta}{2D_\eta}\sin 2\theta_1 & -\dfrac{D_\zeta \cos^2\theta_1 + D_\eta \sin^2\theta_1}{D_\eta}\cos y_4 \end{bmatrix}$$

$$\times\begin{bmatrix} (y_{10} - y_8 \sin y_4)/D_\xi \\ y_{11}/D_\zeta \end{bmatrix}$$

$$y_5' = y_7' - y_3' \sin y_4$$

$$y_6' = (1+y_9)(\cos y_3)\cos y_4 - 1$$

$$y_7' = \frac{y_8}{D_\xi + (D_\eta + D_\zeta)y_9}$$

$$y_8' = (D_\eta - D_\zeta)C_\eta C_\zeta - (J_\eta - J_\zeta)\omega_\eta \omega_\zeta + J_\xi \dot{\omega}_\xi - Q_{\theta_c}$$

$$y_9' = \frac{y_2(\sin\beta)\cos\beta - x\cos^2\beta - 2\dot{y}_1\cos\beta}{EA}$$

$$y_{10}' = (1+y_9)(y_{12}\tan y_3 - y_{13})(\cos y_3)\cos y_4$$
$$+ (J_\xi \omega_\xi T_{12} + J_\eta \omega_\eta T_{22} + J_\zeta \omega_\zeta T_{32})\sin\beta + (J_\xi \omega_\xi T_{13} + J_\eta \omega_\eta T_{23} + J_\zeta \omega_\zeta T_{33})$$

$$y_{11}' = (1+y_9)[y_{14}\cos y_4 - (y_{13}\sin y_3 + y_{12}\cos y_3)\sin y_4]$$
$$- y_3'\left[\frac{y_8}{\cos y_4} - y_{10}\tan y_4\right] + \omega_\xi(J_\eta \omega_\zeta \cos\theta_1 + J_\zeta \omega_\eta \sin\theta_1)$$
$$+ \dot{y}_5(J_\eta \omega_\eta \sin\theta_1 + J_\zeta \omega_\zeta \cos\theta_1) - (J_\zeta \omega_\zeta \sin\theta_1 - J_\eta \omega_\eta \cos\theta_1)$$

$$y_{12}' = \ddot{y}_6 + y_2(\sin\beta)\cos\beta - (x+y_6)\cos^2\beta - 2\dot{y}_1\cos\beta - Q_u$$

$$y_{13}' = \ddot{y}_1 + 2\dot{y}_6\cos\beta - 2\dot{y}_2\sin\beta - y_1 - Q_v$$

$$y_{14}' = \ddot{y}_2 + 2\dot{y}_1\sin\beta + (x+y_6)(\sin\beta)\cos\beta - y_2\sin^2\beta - Q_w$$

$$y_{15}' = y_2\sin^2\beta - (x+y_6)(\sin\beta)\cos\beta. \tag{24}$$

The boundary conditions for the state differential equations, eqn (24), are given below. Since $c < 1/10$ for a typical rotor blade, the homogeneous approximation $G_v(x = 1, \tau = \tau) \approx 0$ is used in order to simplify the integration of the equations. This is done because M_{aero} is proportional to $\gamma c^2/96 < \gamma/9600$, which is less than $1/1000$ for typical values of γ.

$$y_i(0) = = 0 \quad (i = 1, 2, \ldots, 7) \tag{25}$$

$$y_i(1) = = 0 \quad (i = 8, 9, \ldots, 15). \tag{26}$$

Only the first 14 state variables appear in the right-hand side of the state differential equations of motion. The state variable y_{15} is introduced in the formulation with the sole purpose of being able to express the rotor inflow ratio $v_i = \sqrt{C_T/2}$ as shown below.

From the last two equations of eqn (24) it follows that

$$y'_{14e}+y'_{15e} = -Q_{we} \tag{27}$$

and this equation immediately yields

$$\int_0^1 (y'_{14e}+y'_{15e})\,dx \equiv y_{14e}(1)+y_{15e}(1)-y_{14e}(0)-y_{15e}(0) = -\int_0^1 Q_{we}\,dx. \tag{28}$$

Since $y_{14}e(1) = y_{15e}(1) = 0$, the following expression is then obtained for the thrust coefficient after eqns (18) and (28) are combined

$$C_T = \frac{6bc}{\gamma}[y_{14e}(0)+y_{15e}(0)]\cos\beta. \tag{29}$$

Equation (29) provides a convenient way to calculate the inflow ratio $v_i = \sqrt{C_T/2}$ during the iteration process for finding the numerical solution to the state differential equations of motion.

The state variable differential equations of motion admit the equilibrium solution $\underline{y} = \underline{y}_e(x)$. The static equilibrium solution $\underline{y}_e(x)$ can be determined numerically by solving the two-point boundary value problem governed by the resulting ordinary differential equations $\underline{y}'_e(x) = \underline{f}(\underline{y}_e(x))$. By perturbing the equilibrium solution as $\underline{y}(x,\tau) = \underline{y}_e(x)+\varepsilon\underline{y}_s(x,\tau)$, where ε is a "bookkeeping parameter" that is introduced only to keep track of orders of magnitude, expanding the state equation in Taylor series about $\varepsilon = 0$, and truncating the expansion to $O(\varepsilon)$, a set of linearized partial differential equations is obtained. The solution to the linearized differential equations is of the form $\underline{y}_s(x,\tau) = \underline{F}(x)e^{r\tau}$, where $r = \sigma \pm \sqrt{-1}\omega$ is a complex quantity. The resulting linearized differential equations for the 14 components of the column matrix $\underline{F}(x)$ are of the form:

$$\underline{F}'(x) = A(y_e(x);r)\underline{F}(x) \tag{30}$$

where the matrix A is equal to

$$A(\underline{y}_e(x);r) = \left\{\left[I - r\frac{\partial \underline{f}}{\partial \underline{\dot{y}}'} - r^2\frac{\partial \underline{f}}{\partial \underline{\ddot{y}}'}\right]^{-1}\right\}_{\underline{y}=\underline{y}_e}\left[\frac{\partial \underline{f}}{\partial \underline{y}} + r\frac{\partial \underline{f}}{\partial \underline{\dot{y}}} + r^2\frac{\partial \underline{f}}{\partial \underline{\ddot{y}}}\right]_{\underline{y}=\underline{y}_e}. \tag{31}$$

The solution to the linear matrix differential equation (30) for $\underline{F}(x)$ is of the form

$$\underline{F}(x) = \Phi(x)\underline{F}(0) \tag{32}$$

where $\Phi(x)$ is a 14×14 matrix that, in linear system theory, is called the *transition matrix* of the system. By substituting such solution into the differential equation for $\underline{F}(x)$, it is readily seen that the transition matrix satisfies the matrix differential equation

$$\frac{d}{dx}\Phi(x) = A(\underline{y}_e(x);r)\Phi(x) \tag{33}$$

with the initial condition $\Phi(0) = I$, the 14x14 identity matrix.

The eigenvalue r appears in the elements of the transition matrix Φ as an unknown parameter. Such parameter is determined by imposing the boundary conditions at $x = 1$ to the function array $\underline{F}(x)$. To do this, it is convenient to partition $\underline{F}$ as:

Table 1. Parameter values for the plots

c	c_{d0}	γ	EA	J_η	J_ζ
$\pi/40$	0.01	5	200	0	0.000625

$$\underline{F} = [F_1 \ldots F_7 ; F_8 \ldots F_{14}]^T \triangleq \begin{bmatrix} \underline{G}_1 \\ \underline{G}_2 \end{bmatrix}$$

where $\underline{G}_1$ and $\underline{G}_2$ are, respectively, 7×1 column matrices with $\underline{G}_1(0) = \underline{0}$ and $\underline{G}_2(1) = \underline{0}$. By partitioning the transition matrix $\mathbf{\Phi}(x)$ into four 7×7 submatrices, one can then write from eqn (32):

$$\underline{F}(1) = \mathbf{\Phi}(1)\begin{bmatrix} \underline{0} \\ \underline{G}_2(0) \end{bmatrix} \triangleq \begin{bmatrix} \mathbf{\Phi}_{1,1}(1) & \mathbf{\Phi}_{1,2}(1) \\ \mathbf{\Phi}_{2,1}(1) & \mathbf{\Phi}_{2,2}(1) \end{bmatrix}\begin{bmatrix} \underline{0} \\ \underline{G}_2(0) \end{bmatrix} \tag{34}$$

Equation (34) discloses that the condition to have $\underline{G}_2(1) = \underline{0}$ is that the determinant of $\mathbf{\Phi}_{2,2}(1)$ must be equal to zero. Such algebraic condition, which is the *characteristic equation* associated with the equilibrium $\underline{y}_e(x)$, then allows for the eigenvalue(s) r to be determined. There is an infinite number of discrete values of r that satisfies the characteristic equation. The numerical iterations that are necessary to determine the equilibrium solution $\underline{y}_e(x)$, and any desired number of eigenvalues r, were performed using FORTRAN IMSL routines. The results obtained from such calculations are presented and discussed in the next section.

RESULTS AND DISCUSSION

The parameter values that were used to plot the following figures are shown in Table 1. As indicated earlier, all the parameters are non-dimensional quantities. The plots are for a rotor with $b = 4$ blades and with $\beta = 0$ (see Fig. 1).

The values that were used for the normalized stiffnesses D_η and D_ζ are those that yield the values of the *uncoupled flap and lead-lag frequencies* (ω_w^*, ω_v^*) shown in the figure captions. The value used for the normalized torsional stiffness D_ξ corresponds to the *uncoupled torsional frequency* $\omega_\phi^* = 2.5$.

For the sake of completeness, it is worth mentioning how the differential equations of motion for the *uncoupled motions* are obtained. The differential equations for the uncoupled flap and lead-lag motions are, by definition of such motions, obtained by linearizing the second and third of eqn (5) about $v = w = \theta_x = 0$ and neglecting the small effect of the distributed mass moments of inertia in the linearized equations. The differential equation for the uncoupled torsional motion is, by definition of that motion, obtained by setting $v \equiv w \equiv 0$ in the fourth of eqn (5), linearizing the resulting equation about $\theta_x = 0$, and using the approximation $J_\eta = 0$ (therefore, $J_\zeta \equiv J_\xi + J_\eta = J_\xi$), which is an approximation that is valid for a thin rotor blade. For these uncoupled linearized equations, $\beta = 0$ and $\lambda \approx EAe_0 \approx (1-x^2)/2$ (as given by eqns 9 and 21). Very accurate analytical expressions relating such frequencies to the blade's stiffnesses were developed in Peters (1973) using asymptotic expansion methods. The expressions presented in Peters (1973) were used here [and in Crespo da Silva and Hodges (1986b)] to obtain the values of the normalized stiffnesses corresponding to typical values of the uncoupled frequencies used in the helicopter dynamics literature.

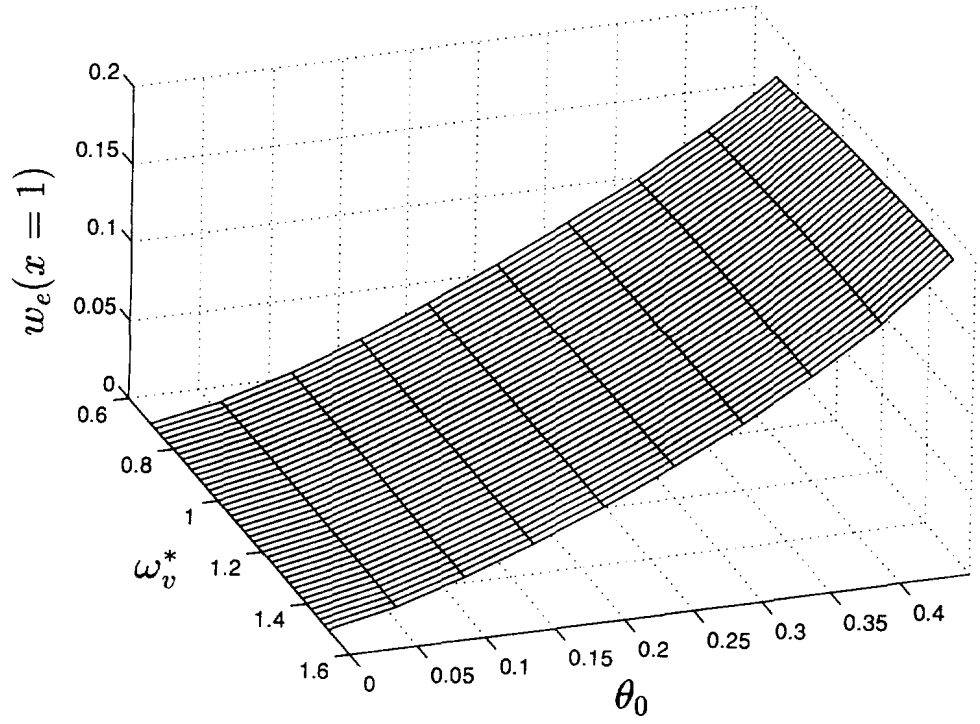

Fig. 3. Flap equilibrium solution at the blade's tip vs ω_r^* and θ_0, for $\omega_w^* = 1.05$.

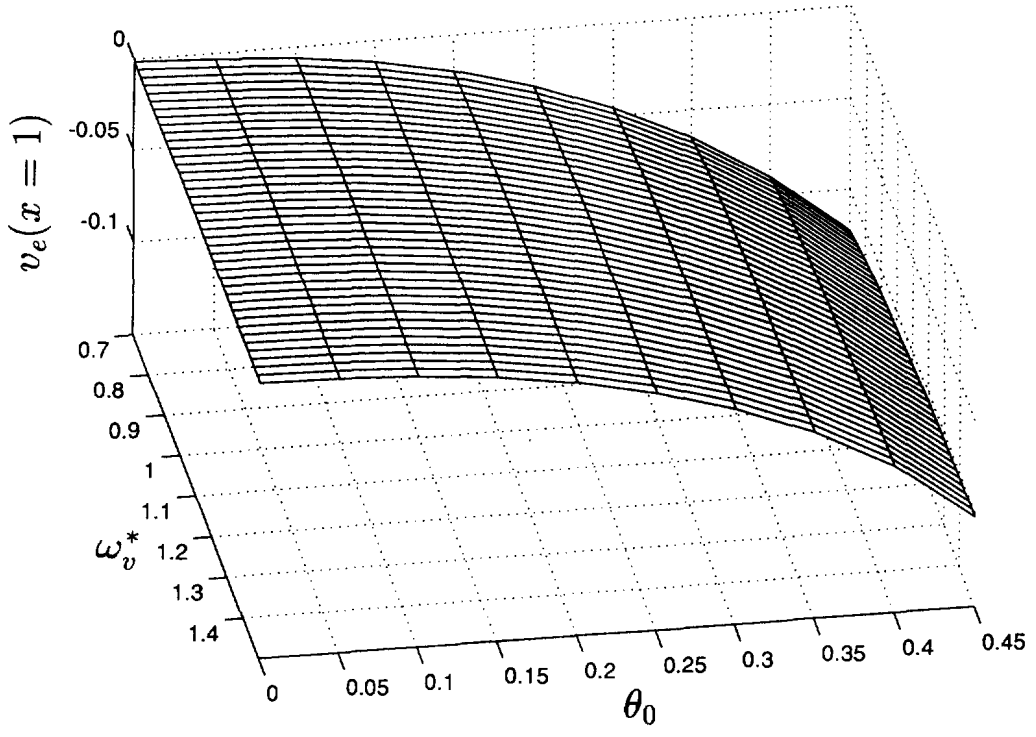

Fig. 4. Lead-lag equilibrium solution at the blade's tip vs ω_r^* and θ_0, for $\omega_w^* = 1.05$.

Figures 3–5 show three-dimensional plots of the static equilibrium solution (w_e, v_e and ϕ_e) at the blade's tip for $\omega_w^* = 1.05$. The values obtained from the numerical integration of the differential equations for the equilibrium correspond to the intersection of any two lines on the surfaces shown in those figures. In those figures (and also in Fig. 6), such points

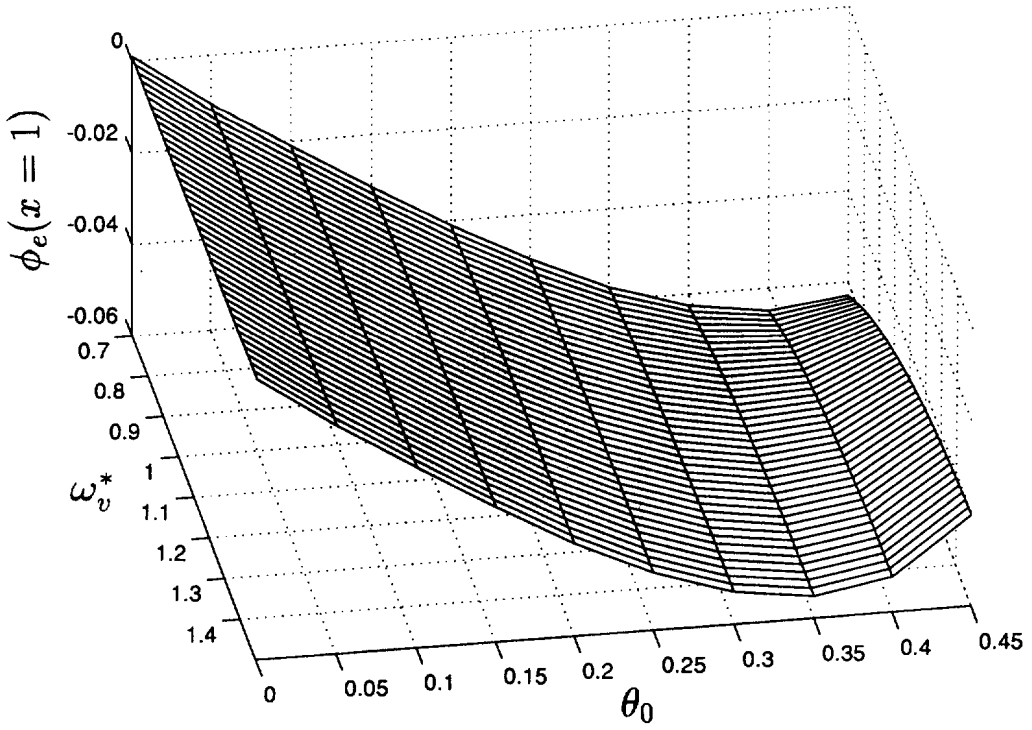

Fig. 5. Torsion angle equilibrium solution at the blade's tip vs ω_v^* and θ_0, for $\omega_w^* = 1.05$.

correspond to $\omega_v^* = 0.7, 0.72, \ldots, 1.5$, and to $\theta_0 = 0, 0.05, \ldots, 0.45$. As the value of the collective pitch angle θ_0 is increased, the aerodynamic lifting force increases and, as a consequence, the blade's upward (i.e. in the $\hat{z}$ direction shown in Fig. 1) flap deflection w_e increases. This is in agreement with the results shown in Fig. 3. As indicated in Figs 4 and 5, an increase in w_e is accompanied by an increase in the blade's lag deflection and by an increase in the magnitude of the blade's angle of twist. Part of the equilibrium surfaces shown in these figures are unstable, as indicated later.

The tip equilibrium solutions for the torsion angle ϕ_e, and for the flap deflection w_e, are shown in Fig. 6 for a stiffer blade with $\omega_w^* = 1.4$. The corresponding lag deflection $v_e(x = 1)$ for the entire range of ω_v^* and θ_0 shown in Fig. 6 is very small. Its maximum magnitude for this stiffer blade is less than 0.03 radians and, for this reason, it is not shown.

Root loci for the first three pairs of eigenvalues $r = \sigma \pm \sqrt{-1}\omega$ associated with the perturbed motion of the blade about its equilibrium are shown in the next three figures. The arrows in each locus indicate how a particular eigenvalue moves in the first and second quadrants of the complex r plane as ω_v^* is changed, with a step equal to 0.02, from $\omega_v^* = 0.7$ to $\omega_v^* = 1.5$ for a particular value of θ_0. Each dot in a locus shown in these figures corresponds to an eigenvalue for a particular value of collective pitch θ_0, and for a value of ω_v^* in the range indicated above and in the figures.

Figure 7 shows the root locus of $0.7 \leqslant \omega_v^* \leqslant 1.5$, with $\theta_0 = 0.35$ and $\omega_w^* = 1.05$. Although the flap and lead-lag motions are coupled, the eigenvalue with the lowest imaginary part ω in that figure is the one that essentially dominates the lightly damped lead-lag v-motion. The eigenvalue that corresponds to the highest frequency in that figure is essentially the one that dominates the torsional motion of the blade. Note that, for the value of θ_0 indicated in the caption for Fig. 7, the real part of one of the eigenvalues becomes positive when ω_v^* reaches a value somewhere between 1.4 and 1.42. When this happens, the equilibrium solution that corresponds to the associated values of the parameters θ_0 and ω_v^* is, of course, unstable. Otherwise, points on the surfaces shown in Figs 3–5 are asymptotically stable.

The root locus for several values of θ_0 changing with a step equal to 0.05 in the range $0 \leqslant \theta_0 \leqslant 0.30$, and for ω_v^* changing with a step equal to 0.02 in the range $0.7 \leqslant \omega_v^* \leqslant 1.5$, is

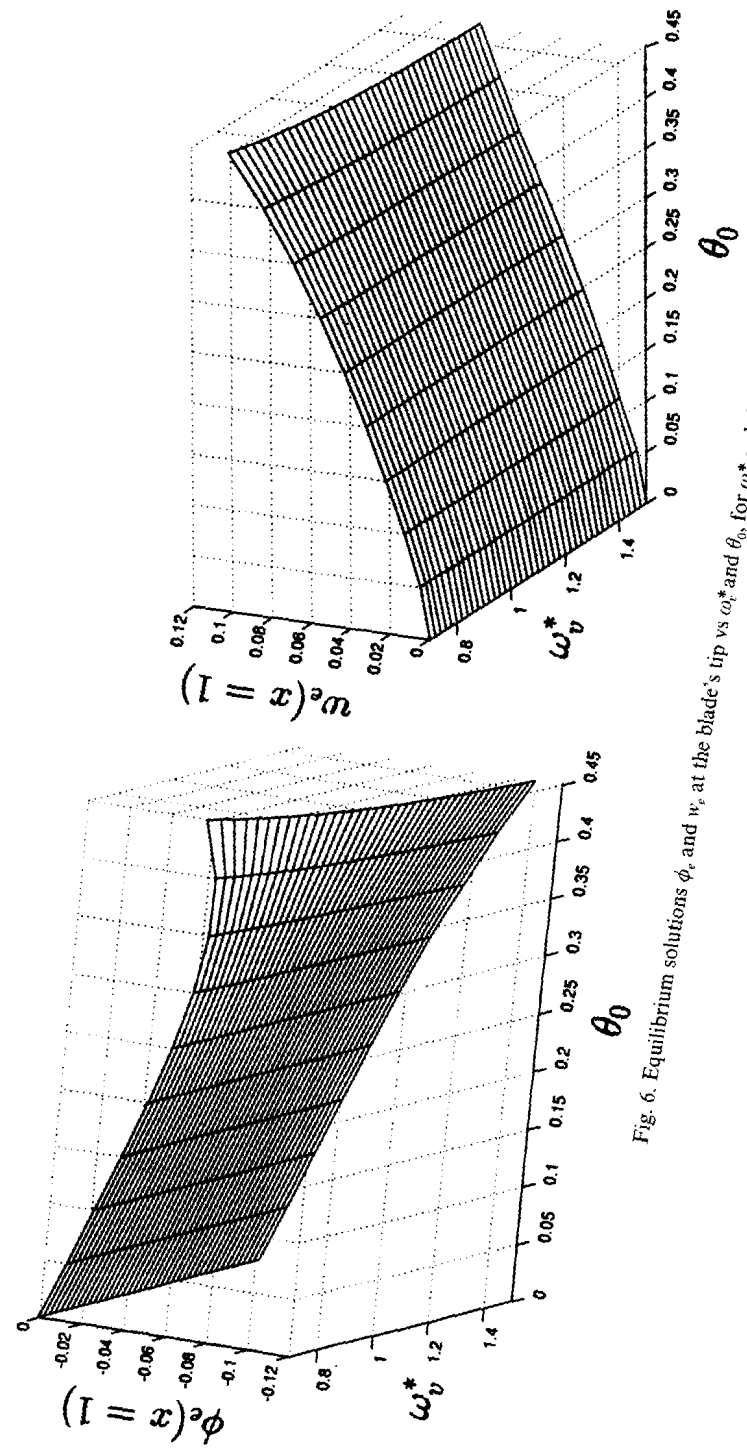

Fig. 6. Equilibrium solutions ϕ_e and w_e at the blade's tip vs ω_t^* and θ_0, for $\omega_*^* = 1.4$.

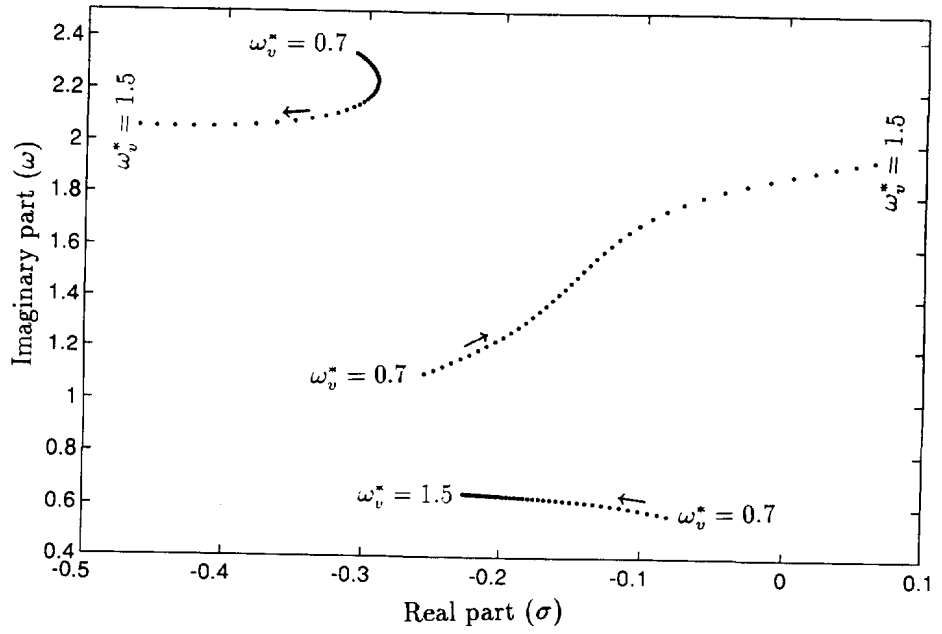

Fig. 7. Root loci for $\omega_w^* = 1.05$, with $\theta_0 = 0.35$ and $0.7 \leqslant \omega_v^* \leqslant 1.5$ (step = 0.02).

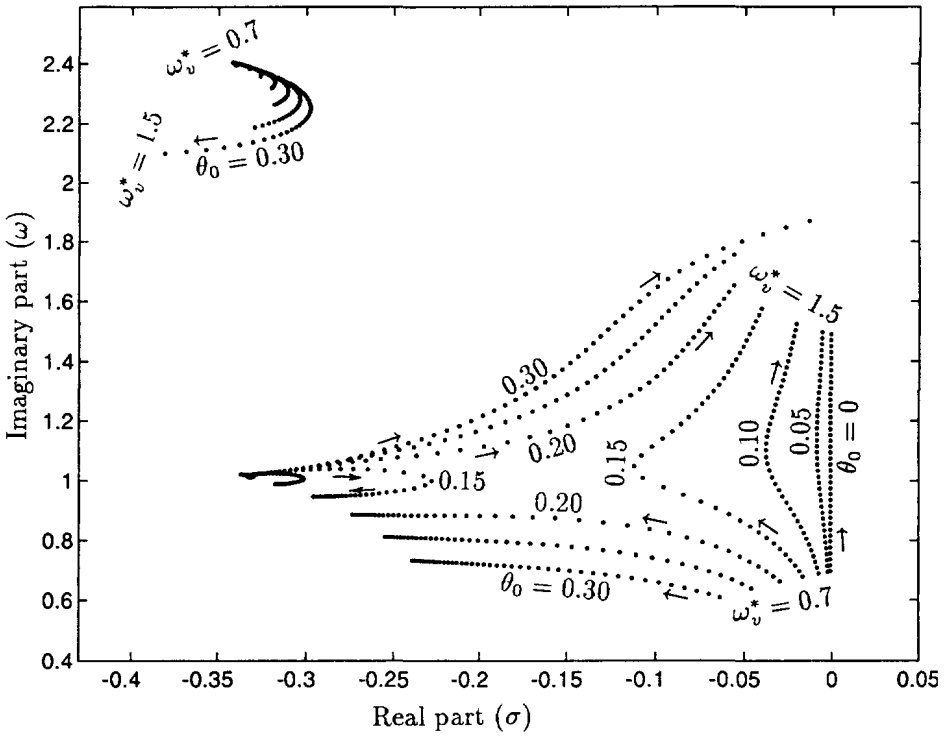

Fig. 8. Root loci for $\omega_w^* = 1.05$, with $0 \leqslant \theta_0 \leqslant 0.3$ (step = 0.05) and $0.7 \leqslant \omega_v^* \leqslant 1.5$ (step = 0.02).

shown in Fig. 8 for $\omega_w^* = 1.05$. All the equilibrium points that correspond to each dot in that figure correspond to an asymptotically stable equilibrium since the real parts of the eigenvalues are negative. Comparing Figs 7 and 8, it is seen that for $\omega_v^* = 1.5$, for example, the blade's equilibrium solution becomes unstable when the collective pitch of all four blades of the helicopter is increased beyond a value that is somewhere between 0.3 and 0.35, but very close to $\theta_0 = 0.3$ (i.e. about 18°).

Root loci associated with the equilibrium solution shown in Fig. 6 for $\omega_w^* = 1.4$ are plotted in Fig. 9 for $\theta_0 = 0$ and $\theta_0 = 0.4$, and for ω_v^* changing in the range $0.7 \leqslant \omega_v^* \leqslant 1.5$

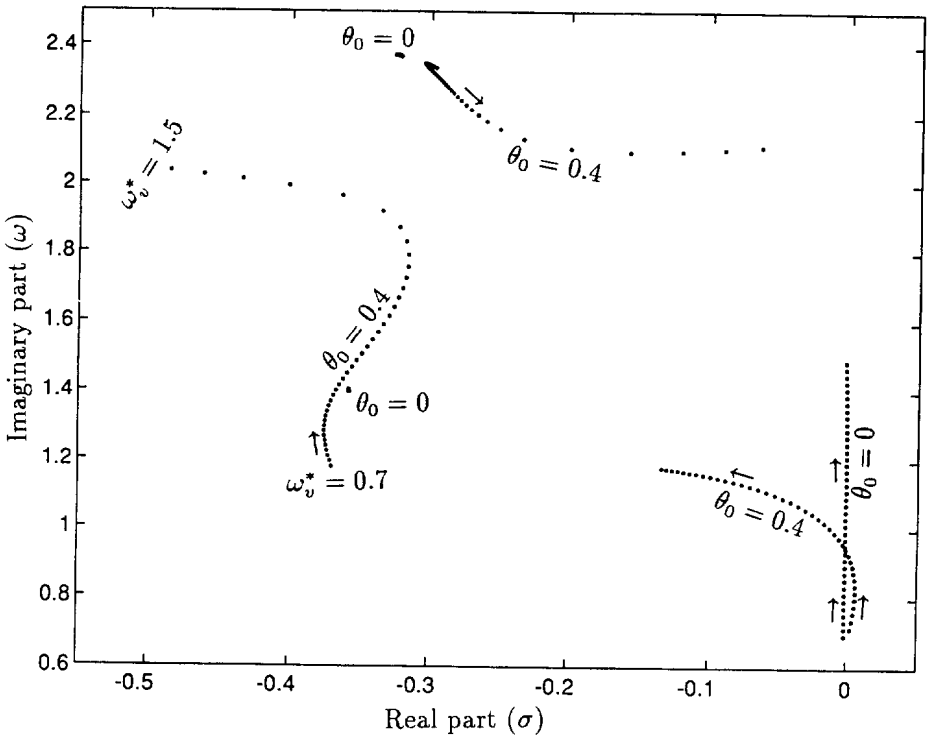

Fig. 9. Root loci for $\omega_v^* = 1.4$, $0.7 \leqslant \omega_r^* \leqslant 1.5$ (step = 0.02) and for $\theta_0 = 0$ and $\theta_0 = 0.4$.

with a step equal to 0.02. For $\theta_0 = 0$, two of the root loci shown in that figure are curves clustered around the points $-0.358+1.4\sqrt{-1}$ and $-0.324+2.374\sqrt{-1}$. For $\theta_0 = 0.4$, those two eigenvalues that were in the clustered loci move in the directions shown by the arrows as ω_r^* is increased from 0.7 to 1.5.

CONCLUDING REMARKS

An analysis methodology that is applicable to all dynamical systems was used to investigate the motion of a helicopter rotor blade. First, the equilibrium solution to the system was obtained by the numerical integration of the nonlinear differential equations of motion. Therefore, the equilibrium solution obtained here could be labeled "numerically exact". By casting the partial differential equations in the form $\underline{y}' = \underline{f}(\underline{y}, \dot{\underline{y}}, \ddot{\underline{y}}, \dot{\underline{y}}', \ddot{\underline{y}}')$, one can determine, with no major difficulty, the mode shapes and the eigenvalues associated with the infinitesimally small perturbations about the equilibrium solution. A substantial amount of data was generated using this methodology, and a number of results were presented in the form of plots showing how the equilibrium solution and the root loci depend on several parameters for the problem that was analyzed.

Approximate results for a similar rotor blade were presented in Crespo da Silva and Hodges (1986b) using expanded equations. When compared to the results obtained here, it is not uncommon to find differences of 20%, for the higher values of collective pitch, between some of those approximate results and the results obtained here. It would be highly desirable if one would, in the future, generate experimental data with the objective of comparing it with the results of the theoretical analysis presented in this paper.

As in other work presented in the rotorcraft literature, the investigation presented here used a simple model for the aerodynamics. It is suggested that further extension of this work make use of more accurate and more realistic aerodynamic models.

It is now well-known that nonlinearities in the differential equations of motion may affect the system dynamics in such way that the actual motion of the system may be quite different from the "linearized motion". This may happen when the system natural frequencies ω_i are related as $|m_1\omega_1+m_2\omega_2+m_3\omega_3+\ldots| \approx 0$, where the m_is are integers.

This phenomenon, which is called "nonlinear resonance", was not addressed here. The root loci presented here disclose a number of possibilities for nonlinear resonances in the motion of a helicopter rotor blade. For example, for $\omega_w^* = 1.05$ and $\theta_0 = 0.15$, two of the eigenvalues associated with the linearized motion are approximately equal to $-0.2325+1.017\sqrt{-1}$ and $-0.1071+1.009\sqrt{-1}$ when $\omega_r^* = 1.02$ (see Fig. 8). Since the frequency ratio for these two eigenvalues is nearly equal to 1 : 1, these modes will likely cause the system to exhibit a nonlinear resonant motion. As disclosed by Figs 8 and 9, the system also exhibits other nonlinear resonances, such as 2 : 1 resonances. To this author's knowledge, neither the importance nor the analysis of such resonant motions, have been addressed in the rotorcraft literature. Since nonlinear resonant motions can be drastically different from the motion predicted by linearization [see, for example, Crespo da Silva and Glynn (1978b); Crespo da Silva and Zaretzky (1994); Zaretzky and Crespo da Silva (1994a, 1994b)], it would be of interest to investigate them analytically and to reinforce such investigations with a set of carefully done experiments with a helicopter rotor. For forward flight, additional resonances caused by the presence of periodic coefficient terms in the differential equations of motion can also be the source of undesirable responses that are not predicted by linearization.

Acknowledgements—The author is indebted to Mr Mark Miller for providing enough computing time that made it possible to generate the substantial amount of data that was used to create the plots shown in this paper. The author dedicates this paper to his colleague and friend for over 30 years, Professor Wolf Altman, from the University of São Paulo in Brazil, in honor of his 70th birthday.

REFERENCES

Bramwell, A. R. S. (1976) *Helicopter Dynamics*, Arnold, London.

Crespo da Silva, M. R. M. (1988) Non-linear flexural-flexural-torsional-extensional dynamics of beams—I. Formulation. *International Journal of Solids and Structures*, **24**(12), 1225–1234.

Crespo da Silva, M. R. M. (1991) Equations for nonlinear analysis of 3D motions of beams. *Applied Mechans Reviews*, **44**(11), Part 2, 51–59.

Crespo da Silva, M. R. M. and Glynn, C. C. (1978a) Nonlinear flexural-flexural-torsional dynamics of inextensional beams. I: Equations of motion. *Journal of Structural Mechanics*, **6**(4), 437–448.

Crespo da Silva, M. R. M. and Glynn, C. C. (1978b) Nonlinear flexural-flexural-torsional dynamics of inextensional beams. II: Forced motions. *Journal of Structural Mechanics*, **6**(4), 449–461.

Crespo da Silva, M. R. M. and Hodges, D. H. (1986a) Nonlinear flexure and Forsion of rotating beams, with application to helicopter rotor blades—I. Formulation. *Vertica*, **102**(2), 151–169.

Crespo da Silva, M. R. M. and Hodges, D. H. (1986b) Nonlinear flexure and torsion of rotating beams, with application to helicopter rotor blades—II. Response and stability results. *Vertica*, **10**(2), 171–186.

Crespo da Silva, M. R. M. and Zaretzky, C. L. (1994) Nonlinear flexural-flexural-torsional interactions in beams including the effect of torsional dynamics. I: Primary resonance. *Nonlinear Dynamics*, **5**, 3–23.

Crespo da Silva, M. R. M., Zaretzky, C. L. and Hodges, D. H. (1991) Effects of approximations on the static and dynamic response of a cantilever with a tip mass. *International Journal of Solids and Structures* **27**(5), 565–583.

Hodges, D. H. and Dowell, E. H. (1974) Nonlinear equations of motion for the elastic bending and torsion of twisted nonuniform blades. NASA TN D-7818.

Hodges, D. H. and Ormiston, R. A. (1976) Stability of elastic bending and torsion of uniform cantilever rotor blades in hover with variable structural coupling. NASA TN D-8192.

Peters, D. A. (1973) An approximate solution for the free vibrations of rotating uniform cantilever beams. NASA TM X-62,299.

Peters, D. A. (1975) Flap-lag stability of helicopter rotor blades in forward flight. *Journal of the American Helicopter Society*, **20**(4), 2–13.

Zaretzky, C. L. and Crespo da Silva, M. R. M. (1994a) Nonlinear flexural-flexural-torsional interactions in beams including the effect of torsional dynamics. II: Combination resonance. *Nonlinear Dynamics*, **5**, 161–180.

Zaretzky, C. L. and Crespo da Silva, M. R. M. (1994b) Experimental investigation of non-linear modal coupling in the response of cantilever beams. *Journal of Sound and Vibration*, **174**(2), 145–167.